Journal of Statistical Physics, Vol. 70, Nos. 3/4, 1993

Crossover and Finite-Size Effects in the (1 + 1)-Dimensional Kardar–Parisi–Zhang Equation

Bruce M. Forrest[1] **and Raúl Toral**[1]

Received April 6, 1992; final May 27, 1992

Crossover scaling of the surface width in the Kardar–Parisi–Zhang equation for surface growth is studied numerically. By means of a perturbative solution of the discretized equation and by comparison with the exact solution of the corresponding linear equation, the finite-size effects due to the spatial discretization are carefully analyzed. The dependence on the nonlinearity of both the finite-size and asymptotic scaling forms is then investigated.

KEY WORDS: Surface growth; crossover effects; finite-size scaling; numerical integration; stochastic differential equations.

1. INTRODUCTION

The Kardar–Parisi–Zhang (KPZ) equation[1] has become widely recognized as a fundamental problem in nonequilibrium statistical mechanics. As a nonlinear generalization of the diffusion equation, it describes many diverse processes in nonequilibrium dynamics. One such process which has attracted considerable attention in recent years is the study of stochastically growing surfaces.[2] In many problems, which include the Eden model[3] and ballistic deposition models,[4] the surface is rough and it is of interest to characterize the behavior of the roughness in terms of a scaling description. It turns out that different growth models[2] are described by the same scaling functions and scaling exponents, suggesting that they belong to the same universality class. One of these universality classes is defined by the prototypical model of Kardar, Parisi, and Zhang.[1] The model describes the time evolution of the (conveniently

[1] Departament de Física, Universitat de les Illes Balears, E-07071 Palma de Mallorca, Spain.
[2] See refs. 5 for recent reviews on kinetic roughening in surface growth models.

0022-4715/93/0200-0703$07.00/0

coarse-grained) height $h(\mathbf{r}, t)$ of the surface at time t above the location $\mathbf{r}$ of a d-dimensional substrate by the KPZ equation:

$$\frac{\partial h}{\partial t} = \nu \nabla^2 h + \frac{\lambda}{2} (\nabla h)^2 + \eta(\mathbf{r}, t) \tag{1.1}$$

Here $\eta(\mathbf{r}, t)$ is a Gaussian random process of mean zero and with correlation function

$$\langle \eta(\mathbf{r}, t)\, \eta(\mathbf{r}', t') \rangle = 2D\delta(\mathbf{r} - \mathbf{r}')\, \delta(t - t') \tag{1.2}$$

The constants ν, λ, and D parametrize surface relaxation, the effects of lateral growth, and the strength of the noise, respectively.

The associated linear ($\lambda = 0$) solution has been obtained,[6] but the equation has so far defied a complete analytical solution in the presence of the nonlinearity which was introduced to account for the tendency of the surface to grow in a direction normal to its local orientation.

A convenient description of the surface roughness is its width $w(t)$, defined in terms of the fluctuations in the surface height:

$$w^2(t) = \langle \overline{h^2} - \bar{h}^2 \rangle \tag{1.3}$$

The bar denotes a spatial average, while the average $\langle \cdots \rangle$ is taken with respect to the random process η. It has now been well established that w follows an asymptotic scaling description in terms of time t and the linear size L of the substrate[7]:

$$w^2(t, L) = L^{2\zeta} F\left(\frac{t}{L^z}\right) = t^{2\beta} \tilde{F}\left(\frac{t}{L^z}\right) \tag{1.4}$$

where ζ and z are the so-called roughness and dynamic exponents, respectively, and where $\beta = \zeta/z$. The function F has the limiting behavior $F(x) \sim x^{2\beta}$ for $x \ll 1$ and approaches a constant for large x.

The exact values of these growth exponents are only known for $d = 1$, where they can be obtained from a fluctuation-dissipation theorem[8] and Galilean invariance[9]: $\zeta = 1/2$, $z = 3/2$, and $\beta = 1/3$. Accurate knowledge of the exponents is important from the point of view that they help identify which microscopic models do indeed belong to the universality class governed by (1.1). Furthermore, they can provide a measure of the accuracy of approximate analytical and numerical solutions of (1.1). However, reliable extraction of accurate estimates for the exponents not only demands careful treatment of finite-size effects, which can limit the surface growth, it also necessitates proper consideration of the crossover from the linear behavior of the surface fluctuations at early times and on

smaller length scales to those characterizing the asymptotic (late-time, nonlinear) behavior. The scaling law (1.4) is only valid in the asymptotic growth regime, where the effects of the nonlinearity have fully developed. There still remains some doubt as to the proper description of this crossover from linear to nonlinear behavior, even for $d=1$, where the asymptotic results are known.

Two such crossover scaling forms have recently been advocated. Although in their original forms they appear to be different, they can both be written in an equivalent form. Grossmann, Guo, and Grant (GGG) proposed[10]

$$w^2(t, L) = t^{2\beta_0} f\left(\frac{t}{L^{z_0}}, \frac{t}{\xi_c^{z_0}}\right) \tag{1.5}$$

while, based on a one-loop renormalization-group (RG) calculation, Nattermann and Tang (NT) found[11]

$$w^2(t, L) = \xi_c^{2\zeta_0} \Phi\left(\frac{t}{t_c}, \frac{L}{\xi_c}\right) \tag{1.6}$$

with $t_c \sim \xi_c^{z_0}$ for $\lambda \ll 1$.

Both involve a crossover length ξ_c. On time scales $t \ll t_c \sim \xi_c^{z_0}$ the growth is characterized by the linear ($\lambda = 0$) exponents ζ_0, β_0, and $z_0 = \zeta_0/\beta_0$. Only for times $t > \xi_c^{z_0}$ do the effects of the nonlinearity become important. Despite their rather differing appearances, both of the above forms fit into the general picture of an extended scaling hypothesis[12] pertaining to multicritical phenomena,[13]

$$w^2(t, L) = L^{2\zeta_0} \mathscr{F}\left(\frac{t}{L^{z_0}}, HL^a\right) = L^{2\zeta_0} \mathscr{F}\left(\frac{t}{L^{z_0}}, \frac{L}{\xi_c}\right) \tag{1.7}$$

where ζ_0 and z_0 are the exponents at the transition point ($\lambda = 0$ here) and where, in this instance, the scaling field[14] is $H = \xi_c^{-1}$, with the associated crossover exponent $a = 1$.

The discrepancy between the two hypotheses lies in the λ dependence of the crossover length. GGG made the Ansatz $t_c \sim \xi_c^{z_0} \sim \lambda^{-\phi}$ and on the basis of their numerical findings were led to conclude $\phi = 3$ in $1+1$ dimensions. The one-loop RG analysis of NT gave a more complicated λ dependence. In $1+1$ dimensions they found the specific expressions

$$\xi_c = a_0 \left| 1 - \left(\frac{\lambda_c}{\lambda}\right)^2 \right|, \qquad t_c = \frac{a_0^{1/2} \xi_c^{3/2} \lambda_c}{2\pi^3 \nu_B \lambda} \tag{1.8}$$

with $\lambda_c = (2\pi^2 \nu_B^3 / D_B a_0)^{1/2}$, where the subscript B denotes the bare values of the parameters and a_0 is the basic length scale of (1.1) (which we will take to be unity, as is usually assumed). In the weak-coupling limit $\lambda \ll \lambda_c$ the NT form becomes $\xi_c \sim \lambda^{-2}$, $t_c \sim \lambda^{-4}$, i.e., the GGG form with $\phi = 4$.

For large enough L ($L \gg \xi_c$, t^{1/z_0}) the growing length scale t^{1/z_0} assumes the role of L and the above scaling forms are replaced by the asymptotic form

$$w^2(t) = t^{2\beta_0} \mathscr{G}\left(\frac{t}{\xi_c^{z_0}}\right) \tag{1.9}$$

Using this form, GGG found a good data collapse with $\xi_c^{z_0} \sim \lambda^{-3}$ and thus inferred $\phi = 3$, in apparent contradiction to the one-loop RG results of Nattermann and Tang.

In this paper we study numerically the crossover behavior from linear to nonlinear dynamics and analyze the results in terms of finite-size-scaling theory. We concentrate on the KPZ equation in $1+1$ dimensions ($d=1$), since there the asymptotic behavior is well known and this therefore provides a convenient test for a numerical solution of the equation. Furthermore, this is obviously the least computationally-intensive case and hence can be studied with the greatest numerical accuracy. Our results indicate that, within the range of parameters accessible to the numerical integration, the proposed asymptotic crossover-scaling forms are indistinguishable. However, the $\phi = 3$ form provides the best description of the observed finite-size crossover-scaling behavior. Great care is taken to analyze the effect of the system size in the simulation.

2. LINEAR THEORY AND PERTURBATION

Before going on to investigate the above scaling forms and attempting to resolve the apparent discrepancy in the findings of GGG and NT, we feel it appropriate, and indeed necessary, to examine the effect of finite L on the solution of the equation.

First of all, we adopt the parametrization proposed in ref. 15 by rescaling $h \mapsto (\nu/2D)^{1/2} h$ and $t \mapsto \nu t$. Then Eq. (1.1) becomes

$$\frac{\partial h(\mathbf{r}, t)}{\partial t} = \nabla^2 h(\mathbf{r}, t) + \frac{\tilde{\lambda}}{2} (\nabla h)^2 + z(\mathbf{r}, t) \tag{2.1}$$

where $\tilde{\lambda} \equiv (2D/\nu^3)^{1/2} \lambda$ and $\langle z(\mathbf{r}, t)\, z(\mathbf{r}', t') \rangle = \delta(\mathbf{r} - \mathbf{r}')\, \delta(t - t')$. This leaves us with only the parameter $\tilde{\lambda}$ to be varied, which is related to the dimensionless coupling constant g by $g = 2\tilde{\lambda}^2$. This parametrization can be achieved simply by fixing $2D = \nu = 1$ and allowing λ to vary.

The discretization which is typically employed in numerically solving (2.1) in $1+1$ dimensions is

$$\frac{\partial h_j(t)}{\partial t} = (h_{j+1} + h_{j-1} - 2h_j) + \frac{\tilde{\lambda}}{2}\left(\frac{h_{j+1} - h_{j-1}}{2}\right)^2 + z_j(t) \tag{2.2}$$

where $j = 1,..., L$ denote the L substrate sites, with analogous forms in higher dimensions. Periodic boundary conditions are imposed. The noise variables satisfy $\langle z_j(t)\, z_{j'}(t')\rangle = \delta_{jj'}\delta(t-t')$.

Although we do not know the exact solution of (2.2), we do have the solution to the corresponding linear ($\tilde{\lambda} = 0$) equation at our disposal.[3] This can easily be obtained by means of a transformation to Fourier space with the discrete Fourier transform

$$\hat{x}_k(t) \equiv \frac{1}{\sqrt{L}} \sum_{j=1}^{L} \exp\left(\frac{2\pi i}{L} jk\right) x_j(t) \qquad (0 \leqslant k \leqslant L-1) \tag{2.3}$$

The mean-square width at time t is given by the general expression

$$w^2(t, L) = \frac{1}{L} \sum_{k=1}^{L-1} \langle \hat{h}_k(t)\, \hat{h}_{-k}(t)\rangle \tag{2.4}$$

[3] This is essentially the *unweighted Gaussian* model solved by Abraham and Upton.[22] Their solution imposed slightly different boundary conditions, namely, $h_{-L}(t) = h_L(t) = 0\ \forall t$ on a lattice of $2L+1$ sites ($-L \leqslant j \leqslant L$).

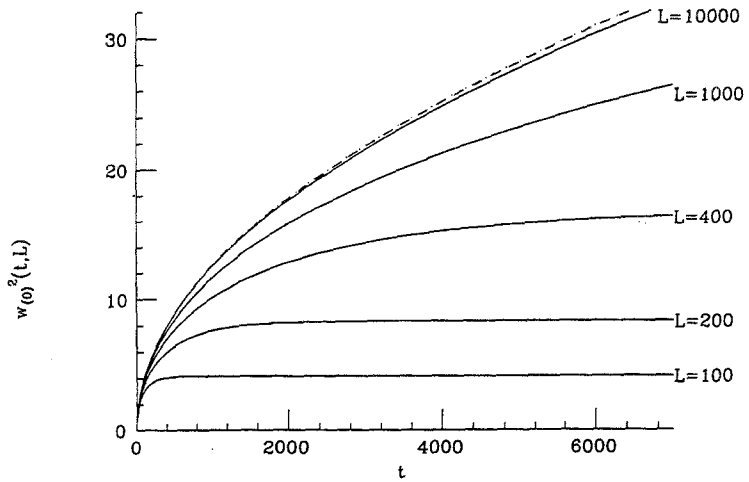

Fig. 1. Mean-square width $w^2_{(0)}$ of the linear solution as a function of time t for various sizes L of the discretization grid. The dashed line is the asymptotic solution (2.7), $L \to \infty$, from the discretized theory. The corresponding solution (2.8) of the continuum theory is given by the dotted line (on the scale shown, the dotted line falls on top of the dashed line).

Substitution of the solution

$$\hat{h}_k(t) = e^{-\alpha_k t} \int_0^t ds\, e^{\alpha_k s} \hat{z}_k(s) \tag{2.5}$$

where $\alpha_k \equiv 4 \sin^2(\pi k/L)$, gives

$$w^2_{(0)}(t, L) = \frac{1}{L} \sum_{k=1}^{L-1} \frac{1 - \exp(-2\alpha_k t)}{2\alpha_k} \tag{2.6}$$

for the width $w_{(0)}(t, L)$ of the linear equation. In Fig. 1 we show $w^2_{(0)}(t, L)$ for various L. It is evident that only for $L \gtrsim 10^4$ does the discretization (2.2) reproduce the asymptotic result accurately (with a relative error in $w_{(0)}$ of 1%) up to times $t \simeq 6000$:

$$w^2_{(0)}(t, L \to \infty) = \frac{1}{\pi} \int_{\pi/L}^{\pi/2} dx \frac{1 - \exp(-8t \sin^2 x)}{4 \sin^2 x} \tag{2.7}$$

In fact, for a substrate of size L the asymptotic result is attained to within 1% only up to time $t_L \simeq 6L^2/10^5$. Hence for a smaller size, such as $L = 1000$, such an accuracy is attained only up to $t \simeq 60$.

Also displayed in the figure is the analogous result

$$w^2_{(0)}(t, L \to \infty) = \frac{1}{\pi} \int_{2\pi/L}^{\pi} dk \frac{1 - \exp(-2k^2 t)}{2k^2} \tag{2.8}$$

from the continuum theory (2.1) at $\tilde{\lambda} = 0$. On the scale shown the results (2.7) and (2.8) are indistinguishable.

The steady-state width in (2.6) is given by

$$w^2_{(0)}(\infty, L) = \frac{1}{L} \sum_{k=1}^{L-1} \frac{1}{2\alpha_k} = \frac{1}{8L} \sum_{k=1}^{L-1} \frac{1}{\sin^2(\pi k/L)} = \frac{L}{24}\left(1 - \frac{1}{L^2}\right) \tag{2.9}$$

while the asymptotic behavior is given to a good approximation (within less than 0.2% for $t \geqslant 1$) by

$$w^2_{(0)}(t, \infty) = \left(\frac{t}{2\pi}\right)^{1/2} \left(1 - \frac{1}{32t}\right) \tag{2.10}$$

These two expressions can be summarized by the scaling form (1.4) with the well-known linear exponents $\zeta_0 = 1/2$, $z_0 = 2$, and $\beta_0 = 1/4$, and where the scaling function is given by

$$F(x) = \frac{1}{4\pi^2} \sum_{k=1}^{\infty} \frac{1 - \exp(-8\pi^2 k^2 x)}{k^2} \tag{2.11}$$

This possesses the limiting behavior $F(x \gg 1) = 1/24 - e^{-8\pi^2 x}/4\pi^2$ and $F(x \ll 1) = (x/2\pi)^{1/2} - x$.

Of course, ensuring that the size L of the grid in (2.2) is large enough to emulate the asymptotic behavior with $\tilde{\lambda}=0$ does not automatically guarantee that it will suffice in the corresponding nonlinear case. However, that this is both a legitimate and desirable precautionary measure is borne out by the following analysis of the discretized nonlinear equation.

In the absence of an exact solution to (2.2) for $\tilde{\lambda}\neq 0$ we can, for sufficiently small $\tilde{\lambda}$, make use of a perturbative solution:

$$h_j(t)=\sum_{n=0}^{\infty}\left(\frac{\tilde{\lambda}}{2}\right)^n h_j^{(n)}(t) \tag{2.12}$$

This yields a recursive solution in Fourier space

$$\hat{h}_k^{(n)}(t)=e^{-\alpha_k t}\int_0^t ds\, e^{\alpha_k s}\hat{f}_k^{(n)}(s) \tag{2.13}$$

with α_k as before, $f_j^{(0)}(t)=z_j(t)$, and

$$f_j^{(n)}(t)=\frac{1}{4}\sum_{m=0}^{n-1}(h_{j+1}^{(n-1-m)}-h_{j-1}^{(n-1-m)})(h_{j+1}^{(m)}-h_{j-1}^{(m)}), \qquad n\geqslant 1 \tag{2.14}$$

We have determined the solution to second order in $\tilde{\lambda}$ (the first-order contribution vanishes, as do all odd orders) as $w_{(0)}^2(t, L)+\tilde{\lambda}^2 w_{(2)}^2(t, L)$ with $w_{(0)}^2(t, L)$ in (2.6) and where, after a straightforward, but tedious calculation,

$$\begin{aligned} w_{(2)}^2(t, L)=\frac{1}{4L^2}\sum_{k=1}^{L-1} e^{-2\alpha_k t}\sum_{k_1=0}^{L-1}\cos^2\left(\frac{\pi(k-k_1)}{L}\right)\Bigg\{&\cos^2\left(\frac{\pi k_1}{L}\right)\\ &\times[f(a, a, t)-f(a, b, t)-f(a, c, t)+f(a, d, t)]\\ &+\cot\left(\frac{\pi k}{L}\right)\sin\left(\frac{2\pi k_1}{L}\right)\\ &\times[f(a, -a, t)-f(a, -b, t)+f(a, c, t)-f(a, d, t)]\Bigg\} \end{aligned} \tag{2.15}$$

where

$$\begin{aligned} a&=-\alpha_{k_1}-\alpha_{k-k_1}+\alpha_k\\ b&=-\alpha_{k_1}+\alpha_{k-k_1}+\alpha_k\\ c&=\alpha_{k_1}-\alpha_{k-k_1}+\alpha_k\\ d&=\alpha_{k_1}+\alpha_{k-k_1}+\alpha_k \end{aligned}$$

$$f(x, y, t)=\frac{xe^{(x+y)t}-(x+y)\,e^{xt}+y}{xy(x+y)}$$

with appropriate limits assumed for $x=0$, $y=0$, and $x+y=0$.

This yields the following contribution to the mean-square steady-state width:

$$w^2_{(2)}(\infty, L) = \frac{1}{4L^2} \sum_{k=1}^{L-1} \sum_{k_1=0}^{L-1} \frac{\cos^2(\pi(k-k_1)/L)}{d(a+d)} \times \left[\cos^2\left(\frac{\pi k_1}{L}\right) - \cot\left(\frac{\pi k}{L}\right) \sin\left(\frac{2\pi k_1}{L}\right) \right] \tag{2.16}$$

We have observed numerically that this varies linearly with L: $w^2_{(2)}(\infty, L) \simeq 1.086 \times 10^{-2} - 6.501 \times 10^{-4} L$ and that the asymptotic behavior of (2.15) also displays a linear dependence: $w^2_{(2)}(t, \infty) = Kt$, where $K \simeq 0.0053$.

Comparing with a numerical solution for $L = 10^4$ (Fig. 2), we see that the perturbative solution, $w^2_{(0)}(t, L) + \tilde{\lambda}^2 w^2_{(2)}(t, L)$, provides a very accurate approximation for $\tilde{\lambda} = 0.5$ up to $t \approx 6000$ and for $\tilde{\lambda} = 1$ for $t \lesssim 1000$.

We can use this perturbative solution at $\tilde{\lambda} = 0.5$ to examine the effect of finite L on the solution in a similar fashion to the linear case studied above. In Fig. 3 we find that, as in the linear case, in order to mimic the asymptotic solution for $w(t)$ up to $t \simeq 6000$ to within an accuracy of 1%,

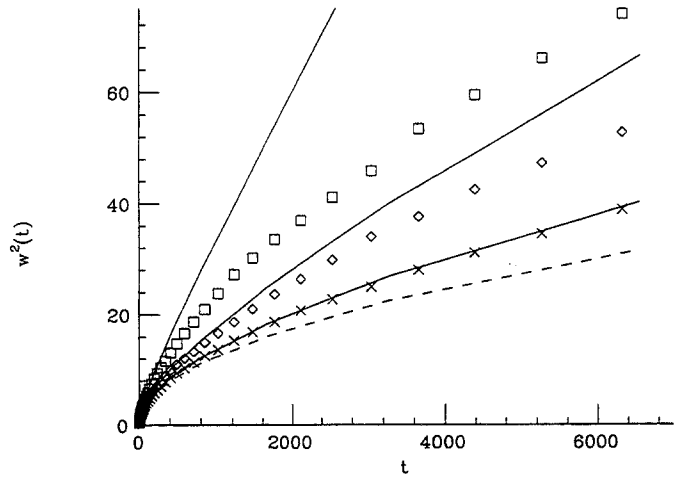

Fig. 2. Comparison of the numerical integration with the perturbative solution to second order in $\tilde{\lambda}$. The symbols denote the numerical solution at $L = 10^4$ with $\tilde{\lambda} = 0.5$ (crosses), $\tilde{\lambda} = 1$ (diamonds), and $\tilde{\lambda} = 2$ (squares). Error bars are smaller than the size of the symbols. The solid lines are the respective results from the perturbative calculation, while the dashed line is the exact linear solution.

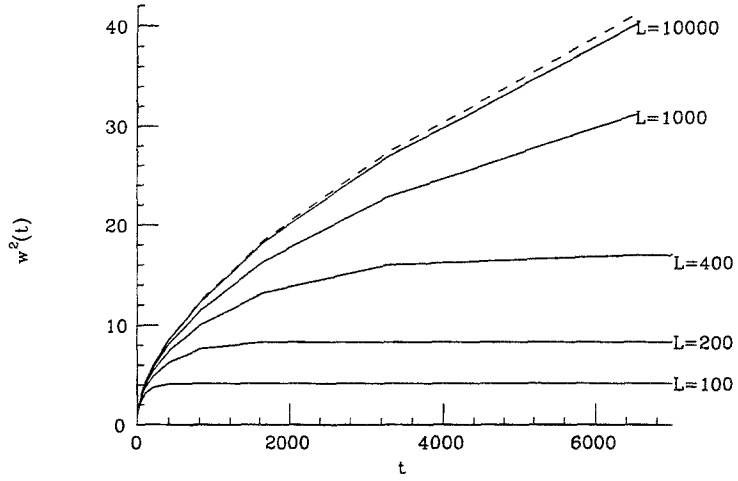

Fig. 3. Finite-size effects in the second-order perturbative solution $w^2(t) = w^2_{(0)}(t) + \tilde{\lambda}^2 w^2_{(2)}(t)$ with $\tilde{\lambda} = 0.5$. The asymptotic solution $L \to \infty$ is given by the dashed curve.

a substrate size of at least $L = 10^4$ is required.[4] In fact, the discrepancy between the finite-L solution and the asymptotic result increases with respect to the $\tilde{\lambda} = 0$ case: e.g., $L = 10^3$ produces a width 10.7% lower than $w(L \to \infty)$ at $t = 6000$ when $\tilde{\lambda} = 0$, but some 13.0% lower with $\tilde{\lambda} = 0.5$. The corresponding values with $L = 10^4$ are 1.0% and 1.2%, respectively. This suggests that the accuracy of the discretization deteriorates upon introduction of the nonlinearity [at least up to $O(\tilde{\lambda}^2)$] and hence that the minimum value of L required in the linear case only provides a lower bound for $\tilde{\lambda} \neq 0$.

With this in mind it is both interesting and instructive to analyze the finite-size dependence of the corresponding discretized linear solution in $2+1$ dimensions,

$$w^2_{(0)}(t, L) = \frac{1}{L^2} \sum_{\substack{k,l=0 \\ (k,l)\neq(0,0)}}^{L-1} \frac{1 - \exp(-2\alpha_k t - 2\alpha_l t)}{2\alpha_k + 2\alpha_l} \tag{2.17}$$

This has a well-known logarithmic dependence[6] $w^2_{(0)} \sim \ln t$ in the asymptotic regime. To test for this behavior, we plot $w^2(2t) - w^2(t)$ versus t in Fig. 4, where a logarithmic time dependence shows up as a constant.

[4] Note that this is purely a systematic error due to finite L. The perturbative solution involves an *exact* stochastic average and an *exact* time integration. When resolving (2.2) numerically one would inevitably introduce statistical uncertainty in addition to a further systematic error due to the time discretization.

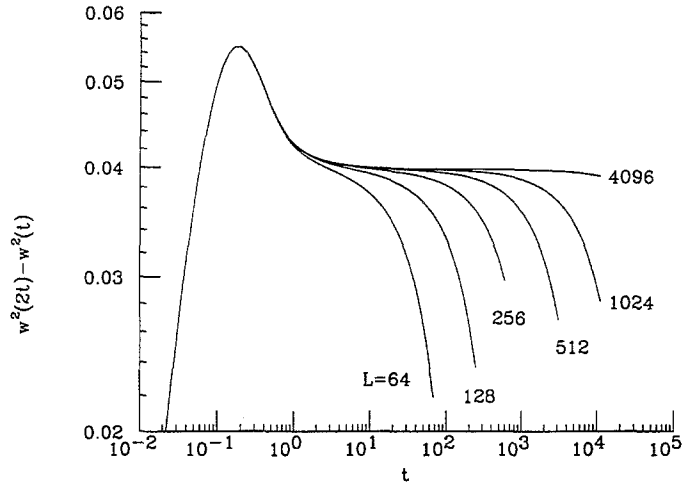

Fig. 4. Size dependence of the linear solution in $2+1$ dimensions for various values of L. Logarithmic behavior corresponds to $w^2(2t)-w^2(t)=\text{const}$.

It can clearly be seen that in order to attain such a behavior a substrate of linear dimension $L \gtrsim 1000$ must be used. This should be contrasted with the much smaller sizes of L already used in the literature, for which no appreciable plateau is visible in Fig. 4. It is not *a priori* clear whether these finite-size effects will be so pronounced with respect to the effective growth exponent β_L for $\tilde{\lambda} \neq 0$, where one has $w^2(t, L) \sim t^{2\beta_L}$. Nevertheless, in view of the L dependence in $1+1$ dimensions one should be cautious when estimating growth exponents on substrates of moderate sizes. We remark here that, using substrates of dimension $L^2 = 128^2$, Chakrabarti and Toral[16] and GGG[10] obtained estimates $\beta_L \simeq 0.13$, while Amar and Family's value[15] of $\beta_L \simeq 0.24$ from systems of size $L^2 = 1024^2$ is much closer to the values obtained in simulations of microscopic models (see Krug and Spohn[5] for a review).

3. NUMERICAL METHOD

In this section we describe the numerical integration of the KPZ equation and the relation of the parametrization (2.1) to others used in the literature.

The parametrization chosen by GGG can be obtained from (2.1) by defining new variables $h_G \equiv (2D)^{1/2} h$, $t_G \equiv \nu t$, and $\lambda_G \equiv \nu\tilde{\lambda}/(2D)^{1/2}$. Since in ref. 10, $2D = 0.01$ and $\nu = 1$, this implies that, in terms of our variables, $h_G = 10h$, $t_G = t$, and $\lambda_G = 10\tilde{\lambda}$. A similar change of scale reproduces the

choice of Moser *et al.*,[17] with $\nu = 1/2$ and $2D = 0.01$, so that $h_M = 10h$, $t_M = t/2$, and $\lambda_M = 5\tilde{\lambda}$. (In terms of the g used in ref. 17 this corresponds to $\tilde{\lambda} = \sqrt{g}$.)

The discretized time-integration scheme which we adopted was a stochastic second-order Runge-Kutta algorithm (Heun method) (e.g., ref. 18). Writing the set of equations (2.1) in general vector form

$$\frac{\partial \mathbf{h}(t)}{\partial t} = \mathbf{F}(\mathbf{h}(t)) + \mathbf{z}(t) \tag{3.1}$$

with the notation $\mathbf{x} \equiv \{x_j;\ j = 1,..., L\}$, the Heun recursion relation prescribes

$$\begin{aligned} \mathbf{g}_1 &= \mathbf{F}(\mathbf{h}(t)) \\ \mathbf{g}_2 &= \mathbf{F}(\mathbf{h}(t) + \Delta t\, \mathbf{g}_1 + (\Delta t)^{1/2}\, \mathbf{u}) \\ \mathbf{h}(t + \Delta t) &= \mathbf{h}(t) + \frac{\Delta t}{2}(\mathbf{g}_1 + \mathbf{g}_2) + (\Delta t)^{1/2}\, \mathbf{u} \end{aligned} \tag{3.2}$$

where the independent random variables $\mathbf{u}$ are Gaussian with mean zero and unit variance.

For the majority of the numerical integrations reported here, we used a step size of $\Delta t = 0.1$. Smaller step sizes did not produce any significant change in the results obtained. As an example, in Fig. 5 we show $w^2(L, t)/L$

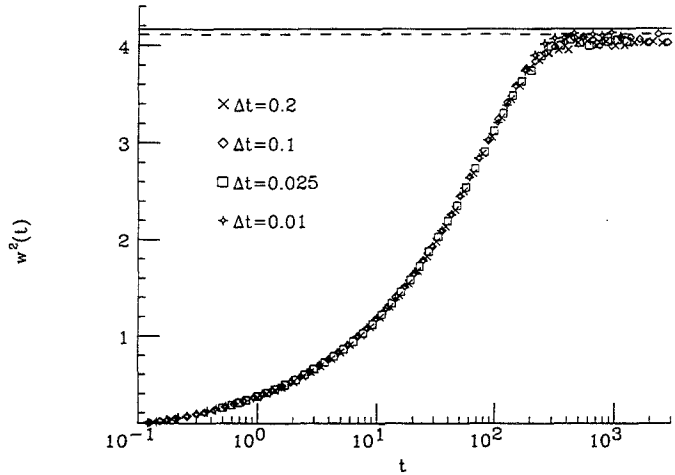

Fig. 5. The step-size dependence of the mean-square width for $\tilde{\lambda} = 1$ and $L = 100$. Each data set was averaged over 5000 independent runs: the resultant error bars are smaller than the symbol sizes. The solid line denotes the steady-state result obtained from the linear theory, while the dashed line includes the correction to $O(\tilde{\lambda}^2)$ from perturbation theory.

as a function of time for $L = 100$ and $\tilde{\lambda} = 1$ with $\Delta t = 0.01$, 0.025, 0.1, and 0.2. The results are seen to be independent of Δt in the presaturation regime, although we detect a slight increase in the equilibrium width with decreasing Δt. Specifically, we find $w^2(\infty, L) = 4.02 \pm 0.01$ for $\Delta t = 0.2$; 4.02 ± 0.01 for $\Delta t = 0.1$; 4.05 ± 0.02 for $\Delta t = 0.025$; and 4.10 ± 0.02 for $\Delta t = 0.01$. The theoretical result from (2.9) for the steady-state width is $w^2_{(0)}(\infty, L) = (L/24)(1 - 1/L^2) = 4.16625$. The numerical integration is seen to fall short of this, but there is a significant $O(\tilde{\lambda}^2)$ correction at $L = 100$. Using (2.16), we obtain $w^2(\infty, L) \simeq w^2_{(0)}(\infty, L) - 0.054\tilde{\lambda}^2 \simeq 4.112$, which is also shown in the figure. Hence, assuming that all higher-order contributions in $\tilde{\lambda}$ are negligible, it would appear that a step size of $\Delta t = 0.01$ or smaller is necessary to obtain the correct equilibrium width, but that larger step sizes suffice in the presaturation regime.

4. ASYMPTOTIC CROSSOVER SCALING

In the light of the foregoing discussion of the effects of finite L on the solution, we used a substrate size of $L = 10^4$ in order to study the asymptotic properties of the solution. A proper investigation of the crossover from linear to nonlinear growth not only demands a sufficiently large L to attain a satisfactory approximation to the asymptotic behavior, but, in addition, one must choose a sensible range of $\tilde{\lambda}$. If $\tilde{\lambda}$ is too small, there will not be enough time to allow development of the nonlinear effects before the finiteness of the substrate saturates the growth fluctuations. On the other hand, a value of $\tilde{\lambda}$ which is too large will result in an almost immediate onset of nonlinear growth upon leaving the diffusive regime, thus excluding any intermediate regime of linear behavior. In Fig. 6 we use the numerical integration in conjunction with the perturbative calculation to order $\tilde{\lambda}^2$ to determine which values of $\tilde{\lambda}$ are appropriate to study the crossover. Despite its deviation from the true behavior at later times, the perturbation serves as a useful indication as to the onset of the nonlinear regime, since we can determine at which time the nonlinear term becomes important. From the figure it can be seen that the diffusive regime persists up until $t \approx 1$ and that $\tilde{\lambda} = 4$ is so large as to obscure any linear regime. We find that only for $0.5 \lesssim \tilde{\lambda} \lesssim 2.5$ is there an appreciable crossover region from linear to nonlinear growth. (We note here that the range of $\tilde{\lambda}$ considered by GGG in $1+1$ dimensions actually corresponds to $0.8 \leqslant \tilde{\lambda} \leqslant 2.2$.)

In Fig. 7 we plot $w^2(t)/\xi_c^{2\zeta_0}$ against t/t_c in order to facilitate a comparison of the two proposed asymptotic scaling forms

$$w^2(t) = t^{2\beta_0} \mathscr{G}(t/\xi_c^{z_0}) \equiv \xi_c^{2\zeta_0} \tilde{f}(t/t_c) \tag{4.1}$$

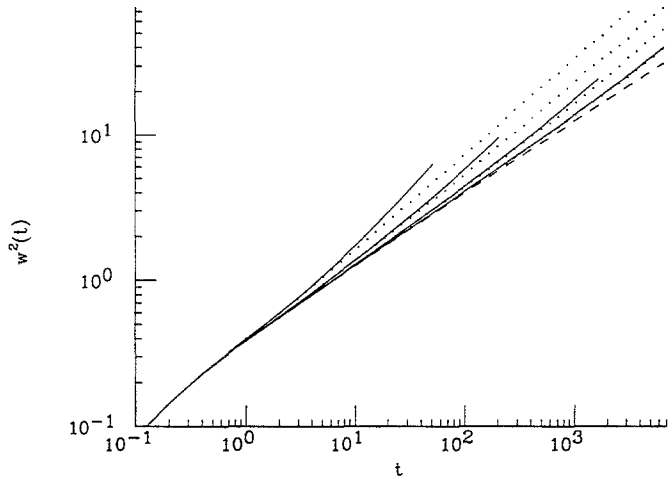

Fig. 6. The effect of the nonlinearity $\tilde{\lambda}$ on the crossover from linear to nonlinear growth. The dashed line is the linear solution: the regime of linear growth $w^2(t) \sim t^{1/2}$ begins at $t \approx 1$. The solid lines are $w^2_{(0)}(t) + \tilde{\lambda}^2 w^2_{(2)}(t)$ with, from bottom to top, $\tilde{\lambda} = 0.5$, 1.0, 2.0, and 4.0. The respective numerically integrated solutions are given by the dots.

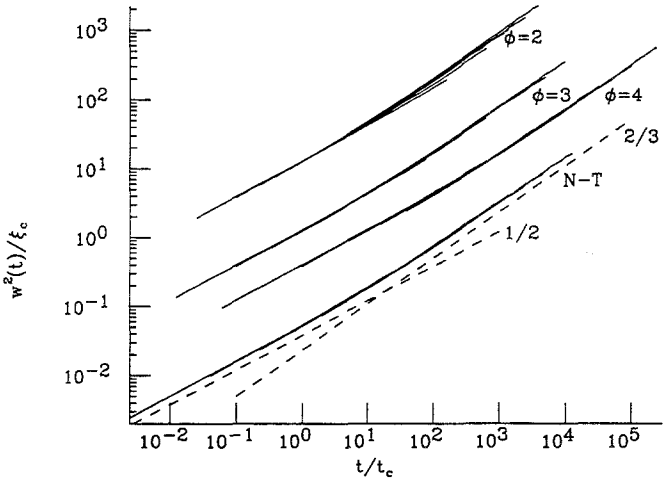

Fig. 7. The asymptotic crossover-scaling forms with $\tilde{\lambda} = 0.5$, 1.0, 1.5, 2.0, and 2.5. The dashed lines depict the two limiting behaviors of linear growth $w^2(t) \sim t^{1/2}$ and nonlinear growth $w^2(t) \sim t^{2/3}$. Error bars have been omitted and the data sets with $\phi = 2$ and $\phi = 3$ have been shifted by constant amounts parallel to the axes in the interests of clarity.

with the GGG hypothesis given by $t_\varepsilon \sim \xi_c^{z_0} \sim \tilde{\lambda}^{-\phi}$ and where the NT form uses ξ_c and t_c in (1.8). We only show data for $t > 1$, since for $t \lesssim 1$ the system exhibits diffusive behavior $w^2(t) \sim t$. We display the data on a logarithmic time scale to expose the whole of the time range. Each data set is averaged over 100 independent runs.

Both the NT form and the GGG form with $\phi = 3$ and $\phi = 4$ provide a good data collapse, while the data with, e.g., $\phi = 2$ do not scale. Within the accuracy of the data it seems impossible to distinguish between the two proposed forms. We also find that removing the slope 1/2 from the curves by plotting $w^2(t)/[\xi_c^{2\zeta_0}(t/t_c)^{1/2}]$ against t/t_c does not help resolve the situation. In view of this and considering the limitations imposed by the finite discretization (even at $L = 10^4$), it appears that a computational effort orders of magnitude greater would be required in order to determine the correct scaling form. In this respect we find no real contradiction between the findings of GGG and the RG calculation of NT.

We note here that, using their numerical data, GGG were able to differentiate between $\phi = 3$ and $\phi = 4$, but that their results were obtained using $L = 10^3$ up to $t = 10^4$. It appears evident from Figs. 1 and 3 that at this system size there are clear finite-size effects.

It is interesting to compare the above three scaling forms for the mean-square width calculated from second-order perturbation theory, $w^2(t) \simeq w_{(0)}^2(t) + \tilde{\lambda}^2 w_{(2)}^2(t)$. For this (see Fig. 8) the NT and $\phi = 4$ forms give the better scaling description. Indeed, for small values of $\tilde{\lambda}$, one would

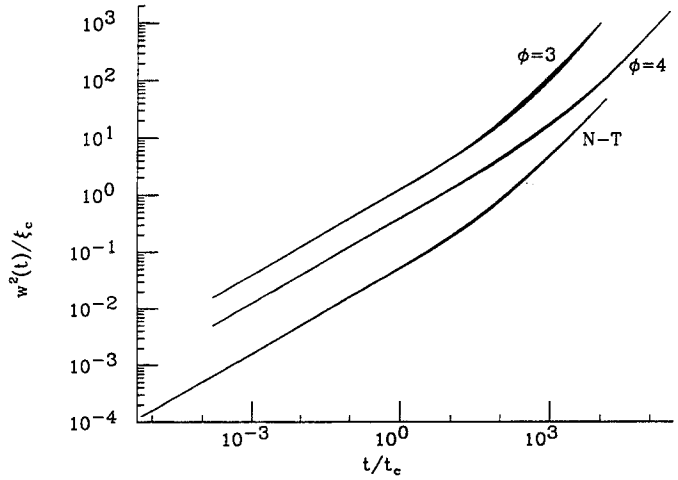

Fig. 8. A test of the asymptotic crossover scaling using the result of the second-order perturbation theory. The range of $\tilde{\lambda}$ used is $0.5 \leqslant \tilde{\lambda} \leqslant 2.5$.

expect the result $\phi = 4$ from the perturbation theory, since it can be obtained from a simple scaling argument[10] which assumes that none of the parameters ν, λ, or D is renormalized. At small enough $\tilde{\lambda}$ (weak nonlinearity) the renormalized parameters ν and D remain close to their bare values, so that this assumption is approximately valid.

5. FINITE-SIZE CROSSOVER SCALING

We can incorporate the limitations due to the finite extent of the substrate by considering the crossover scaling for finite L. In general (1.7) may be written as

$$w^2(t, L) = L^{2\zeta_0} f\left(\frac{t}{t_c}, \frac{L}{\xi_c}\right) \tag{5.1}$$

We consider the nonlinear-to-saturation regime where the crossover to nonlinear growth has already taken place: $t \gg t_c$. In order to observe this, the substrate size must be large enough so that saturation effects occur much later than the crossover to nonlinear growth: $L^{z_0} \gg t_c$, i.e., one must have $L \gg \xi_c$. In this nonlinear-to-saturation regime ($t \gg t_c$, $L \gg \xi_c$), Eq. (5.1) must reduce to the general form

$$w^2(t \gg t_c, L \gg \xi_c) = L^{2\zeta} F\left(\frac{t}{L^z}\right) \tag{5.2}$$

Since $\zeta_0 = \zeta$ ($= 1/2$) in $1+1$ dimensions, from (5.1) and (5.2) we thus have

$$w^2(t \gg t_c, L \gg \xi_c) = L^{2\zeta} \tilde{F}\left(\frac{t}{t_c} \times \frac{\xi_c^z}{L^z}\right) \tag{5.3}$$

The GGG conjecture hence becomes

$$w_{\mathrm{G}}^2(t \gg t_c, L \gg \xi_c) = L^{2\zeta} f_{\mathrm{G}}\left(\lambda^{\phi(1 - z/z_0)} \frac{t}{L^z}\right) \equiv L f_{\mathrm{G}}\left(\tilde{\lambda}^{\phi/4} \frac{t}{L^{3/2}}\right) \tag{5.4}$$

while the NT form is

$$w_{\mathrm{NT}}^2(t \gg t_c, L \gg \xi_c) = L^{2\zeta} f_{\mathrm{NT}}\left(\frac{2\pi^3 \nu_B}{a_0^{1/2} \lambda_c} \lambda \frac{t}{L^z}\right) \equiv L \tilde{f}_{\mathrm{NT}}\left(\tilde{\lambda} \frac{t}{L^{3/2}}\right) \tag{5.5}$$

which is equivalent to (5.4) with $\phi = 4$. This $\phi = 4$ form also agrees with the expression

$$w^2(L, t) = (D/\nu)\, L f(|\lambda|\, (D/\nu)^{1/2}\, t/L^{3/2})$$

recently postulated by Amar and Family[19] and with the findings of Krug *et al.*[20] Hwa and Frey[21] have recently derived a scaling form for the

steady-state height–height correlation function, $C(r, t) = Ar^{2\zeta}F(\lambda\sqrt{A}\, t/r^z)$, which would also appear to lend support to the hypothesis $\phi = 4$.

Hence in this scaling regime we need only consider the form given by (5.4). However, we should only use those data which correspond to this regime, i.e., those satisfying (5.2). In Fig. 9a we display the data scaled according to (5.2). For a given value of $\tilde{\lambda}$ the curves for different L collapse onto a single master curve. In Fig. 9b we then attempt to collapse this

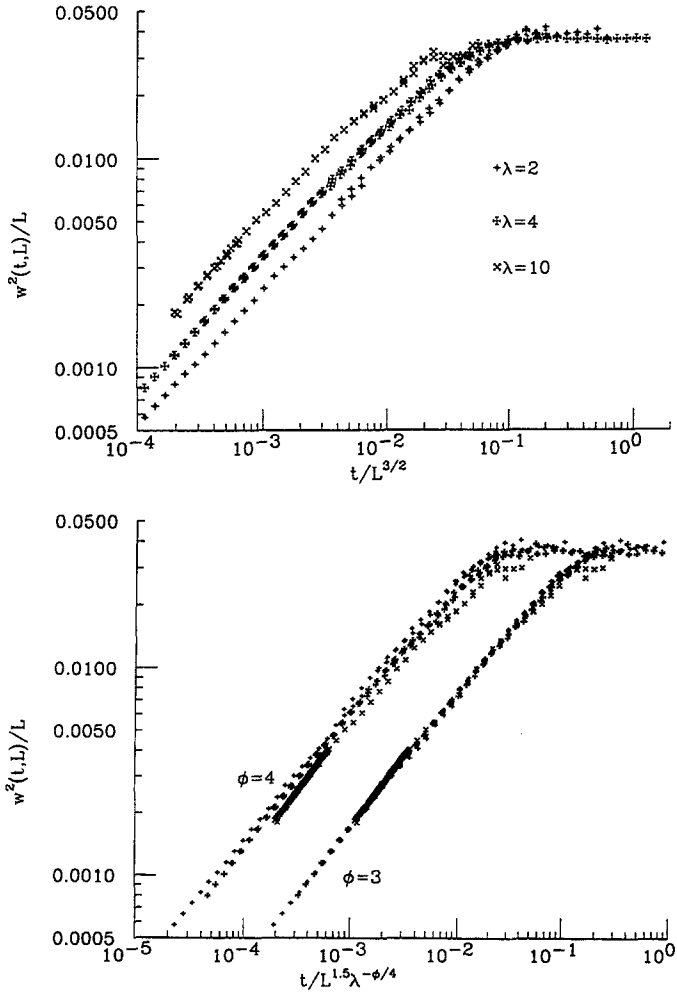

Fig. 9. (a) Finite-size scaling for system sizes $L = 100$, 500, 1000, and 10000. (b) The corresponding scaling forms including the $\tilde{\lambda}$ dependence, with the same symbols as in (a). For purposes of clarity the data set with $\phi = 4$ has been shifted parallel to the horizontal axis. The symbol sizes indicate the order of magnitude of the statistical errors.

family of master curves, parametrized by $\tilde{\lambda}$, onto a universal scaling curve described by (5.4). The choice of $\phi = 3$ appears to give a significantly superior data collapse to that of $\phi = 4$.

6. DISCUSSION

The reason for the failure of the NT form to produce a satisfactory data collapse for finite L could be that, first, the specific expressions (1.8) derived from the one-loop RG analysis are only strictly valid in the $L \to \infty$ limit, and, second, the values of $\tilde{\lambda}$ used here are quite large ($2 \leqslant \tilde{\lambda} \leqslant 10$)—the one-loop RG expansion should be valid for small values of $\tilde{\lambda}$.

One might also question the assumption that the input parameters D, ν, and λ in the discretized KPZ equation actually correspond to the bare parameters used in an RG calculation. The latter may conceivably be affected by the spatiotemporal discretization. We note here that the discrete and continuous models give results for the equilibrium width which differ quantitatively: from the discretized theory (2.9) one obtains $w^2_{(0)}(\infty, L \gg 1) = L/24$, while the continuous theory (2.7) identifies L with the lower cutoff in the momentum integration, giving $w^2_{(0)}(\infty, L \gg 1) = L/4\pi^2$. In this respect there will always be a discrepancy between the continuous and discrete models, no matter how large L is.

However, we do not feel that the bare values in (1.1) are significantly altered to such an extent as to affect the scaling forms tested here—using the expressions derived from the RG analysis and directly substituting the input parameters for the bare values resulted in a good scaling description of our data. Moreover, the scaling relation (5.5) does not contain any specific reference to the value of the parameters ν and D. Any variation in these parameters would only multiply $\tilde{\lambda}$ by a constant value and the scaling form (5.5) would remain intact.

In summary, we find that, while we cannot find any significant difference in the quality of asymptotic crossover scaling among the forms which we tested, we find that the $\phi = 3$ form provides the best scaling description of the crossover behavior for finite systems. We have also highlighted the importance of carefully considering finite-size effects in the discretized solution when attempting to study asymptotic behavior. We have shown that, at least in $1 + 1$ dimensions and possibly in higher dimensions, comparison with the exactly obtainable linear solution can help provide a lower bound on L. Comparison with both the linear solution and the perturbative nonlinear solution can also prove valuable when identifying the crossover regime and the values of the nonlinearity $\tilde{\lambda}$ appropriate to its study.

ACKNOWLEDGMENTS

Financial support from the Dirección General de Investigación Científica y Técnica grant PB89-0424 is gratefully acknowledged. We would also like to thank L.-H. Tang, H. Guo, and E. Hernández for a critical reading of the manuscript. B.M.F. is supported by a grant from the Ministerio de Educación y Ciencia.

REFERENCES

1. M. Kardar, G. Parisi, and Y.-C. Zhang, *Phys. Rev. Lett.* **56**:889 (1986); E. Medina, T. Hwa, M. Kardar, and Y.-C. Zhang, *Phys. Rev. A* **39**:3053 (1989).
2. M. Lagally, ed., *Kinetics of Ordering and Growth at Surfaces* (Plenum Press, New York, 1990), and references therein; T. R. Thomas, *Rough Surfaces* (Longman, London, 1982).
3. M. Eden, in *Symposium on Information Theory in Biology*, H. P. Yockey, ed. (Pergamon Press, New York, 1958), p. 359.
4. M. J. Vold, *J. Colloid Sci.* **14**:168 (1959).
5. F. Family and T. Vicsek, eds., *Dynamics of Fractal Surfaces* (World Scientific, Singapore, 1991); J. Krug and H. Spohn, in *Solids Far From Equilibrium: Growth, Morphology and Defects*, C. Godrèche, ed. (Cambridge University Press, Cambridge, 1991); L. Sander, in *Solids Far From Equilibrium: Growth, Morphology and Defects*, C. Godrèche, ed. (Cambridge University Press, Cambridge, 1991); D. E. Wolf, in *Kinetics of Ordering and Growth at Surfaces*, M. Lagally, ed. (Plenum Press, New York, 1990); F. Family, *Physica A* **168**:561 (1990); T. Vicsek, *Fractal Growth Phenomena* (World Scientific, Singapore, 1989).
6. S. F. Edwards and D. R. Wilkinsons, *Proc. R. Soc. Lond. A* **381**:17 (1982).
7. F. Family and T. Vicsek, *J. Phys. A* **18**:L75 (1985); R. Jullien and R. Botet, *J. Phys. A* **18**:2279 (1985).
8. U. Dekker and F. Haake, *Phys. Rev. A* **11**:2043 (1975).
9. P. Meakin, P. Ramanlal, L. M. Sander, and R. C. Ball, *Phys. Rev. A* **34**:5091 (1986); J. Krug, *Phys. Rev. A* **36**:5465 (1987).
10. B. Grossmann, H. Guo, and M. Grant, *Phys. Rev. A* **43**:1727 (1991).
11. T. Nattermann and L.-H. Tang, *Phys. Rev. A* **45**:7156 (1992).
12. J. Kertész and D. E. Wolf, *Phys. Rev. Lett.* **62**:2571 (1989); L.-H. Tang, T. Nattermann, and B. M. Forrest, *Phys. Rev. Lett.* **65**:2422 (1990).
13. M. E. Fisher, *Rev. Mod. Phys.* **46**:597 (1974) and references therein.
14. R. B. Griffiths, *Phys. Rev. Lett.* **24**:715 (1970).
15. J. G. Amar and F. Family, *Phys. Rev. A* **41**:3399 (1990).
16. A. Chakrabarti and R. Toral, *Phys. Rev. B* **40**:11419 (1989).
17. K. Moser, J. Kertész, and D. E. Wolf, *Physica A* **178**:215 (1991).
18. C. C. Gard, *Introduction to Stochastic Differential Equations* (Marcel Dekker, New York).
19. J. G. Amar and F. Family, *Phys. Rev. A* **45**:R3373 (1992).
20. J. Krug, P. Meakin, and T. Halpin-Healey, *Phys. Rev. A* **45**:638 (1992).
21. T. Hwa and E. Frey, *Phys. Rev. A* **44**:R7873 (1991).
22. D. B. Abraham and P. J. Upton, *Phys. Rev. B* **39**:736 (1989).